Plasmonics (2023) 18:283–289
https://doi.org/10.1007/s11468-022-01766-w

Synthesis of Magnetic Plasmonic Au/AgAu Heterostructures with Tunable Gap Width for Enhancing Raman Performance

Zhi-Rui Zhao[1] · Shuo Zhang[1] · Rui-Ping Jing[1] · Hao-Sen Kang[2] · Si-Jing Ding[1] · Liang Ma[2]

Received: 10 November 2022 / Accepted: 8 December 2022 / Published online: 20 December 2022

Abstract

For noble metal core–shell nanomaterials with gaps, inserting Raman reporter molecules into the gaps allows for great Raman enhancement and has found promising applications in molecular analysis, bioimaging, and other fields. Herein, we synthesized Au/AgAu core–shell nanostructures with rhodamine B molecules encapsulated in the nanogap. Au/AgAu heterostructures have magnetic plasmon resonance by selecting gold nanocups as the substrate and tunable gap width by adjusting the molar ratio between Au and Ag during growing the shell. The strong and adjustable plasmon coupling between the core and the shell results in prominent electromagnetic field enhancement. Under the synergistic effect of electromagnetic plasmon resonance and plasmon coupling, the Au/AgAu heterostructures show excellent surface Raman scattering signal. Au/AgAu core–shell nanostructures with ~ 3.2 nm nanogap width display the highest Raman intensity. As the gap width is further reduced, the Raman signal gradually decreases, which may be due to the fact that the thicker alloy shell weakens the light penetration and scattering. Our findings can provide the inspiration for synthesize gap-enhanced Raman tags based on magnetic plasmon coupling.

Keywords Au/AgAu heterostructures · Electromagnetic plasmon resonance · Plasmon coupling · SERS

Introduction

Raman scattering spectroscopy can offer the information of molecular vibration and rotation, and it is a qualitative and quantitative analysis method that can be widely used in various scientific fields and daily life [1–5]. However, the signal of Raman scattering is too weak to be observed [6], and people have been exploring various ways to enhance the Raman scattering signal. The methods of enhancing Raman scattering mainly include surface-enhanced resonance Raman scattering (SERRS), coherent anti-Stokes Raman scattering (CARS), and surface-enhanced Raman scattering (SERS) [7–14]. SERS is a phenomenon associated with significant amplification of the Raman signals of analytes located near the surface of signal-enhancing materials, and people usually improve Raman performance by combining the plasmon coupling of noble metal nanomaterials. SERS based on noble metal nanomaterials can be applied in molecular analysis, material characterization, and other fields [15–19]. Various forms of Raman signal enhancement can be easily achieved by changing the plasmon properties, and the plasmon characteristics are controllable by changing the morphology, size, structure, and composition of noble metal nanomaterials [20–26].

For SERS based on plasmon coupling of noble metal nanomaterials, the main enhanced physical mechanism is the local electric field enhancement due to plasmon coupling and hot spots [13, 27–31]. Therefore, the design and preparation of noble metal nanostructures with strong electromagnetic fields and abundant hot spots is the key to achieve surface Raman enhancement [32–38]. Ding's research group et al. reported that gold nanorods with tunable surface roughness were obtained with all-surround hot spots to achieve SERS [32]. Lin et al. reported an Au@Ag core–shell nanocube with fine-tuned edge length as SERS substrate for Raman enhancement [33]. Ye et al. reported that a kind of Au–Ag hybrid multi-shell nanoparticles enhanced the SERS

✉ Si-Jing Ding
dingsijing@cug.edu.cn

✉ Liang Ma
maliang@wit.edu.cn

[1] School of Mathematics and Physics, China University of Geosciences (Wuhan), Wuhan 430074, People's Republic of China

[2] Hubei Key Laboratory of Optical Information and Pattern Recognition, Wuhan Institute of Technology, Wuhan 430205, People's Republic of China

performance of the NPs [34]. Furthermore, researchers have found that the nanogap in the interior can make Raman molecules almost not be affected by the external environment, as well as Raman molecules will be subjected to uniform and stably enhanced electromagnetic fields in the interior of the nanogap [39–46]. Ma's team reported that Au/AgAu hybrids with adjustable gap width and counts were synthesized by controllable galvanic replacement based on Au nanospheres and achieved outstanding SERS response [39]. Zhang's research group prepared Au/AgAu core–shell nanorods with Raman reporters embedded in the nanogap, which generated strongly enhanced and stable Raman signals [40]. Zhao et al. reported gap-tethered SERS-active Au@AgAu nanoparticles serving as Raman tags for the detection of MC-LR at a very low concentration [41].

However, in previous work, most nanostructures only exhibit electric field enhancement, and there are few reports of magnetic field enhancements. In this work, Au/AgAu core–shell nanostructures have not only electric but also magnetic plasmon resonance by selecting gold nanocups as the substrate. The gap width between the core and shell is tunable by adjusting the molar ratio of Au to Ag during growing the shell. The prepared Au/AgAu core–shell nanostructures have tunable plasmon resonance and strong electromagnetic field, which yield Au/AgAu core–shell nanostructures with improved and controllable SERS signals. Subsequently, the physical mechanism of Raman signal enhancement is discussed.

Material and Methods

Materials

Cetyltrimethylammonium bromide (CTAB, 99.0%) and N-hexadecyltrimethylammonium chloride (CTAC, 99.0%) were obtained from Aladdin. Thioacetamide (TAA, 99.0%), lead acetate ($Pb(Ac)_2$, 99.5%), L-ascorbic acid (AA, 99.7%), chloroauric acid ($HAuCl_4{\cdot}4H_2O$, 99.0%), and silver nitrate ($AgNO_3$, 99.5%) were bought from Sinopharm Chemical Reagent Co. Ltd. (Shanghai, China). Deionized water with a resistivity of about 18.2 MΩ·cm was used as the solvent in all experiments.

Synthesis of Rhodamine B (RhB)-Modified Gold Nanocups with Ag Shell (Au/Ag Nanocrystals)

Gold nanocups were prepared by selective growth of gold on PbS nanooctahedra and subsequent selective dissolution of the PbS component [47]. The as-prepared gold nanocups (2 mL) were mixed with RhB aqueous solution (2×10^{-4} M, 2 mL) and shaken for 4 h. The RhB-modified gold nanocups were centrifuged at 4500 rpm for 5 min and redispersed in deionized water (2 mL). Subsequently, CTAC (0.3 mL, 0.2 M) and CTAB (0.2 mL, 0.2 M) were added to 2 mL RhB-modified gold nanocups and heated with magnetic stirring at 60 °C for 10 min. Afterwards, the pre-prepared solution A ($AgNO_3$ (0.08 mL, 0.01 M) and deionized water (1 mL)) and solution B (CTAC (0.2 mL, 0.2 M), AA (0.3 mL, 0.1 M) and deionized water (0.5 mL)) were slowly and alternately injected into the pre-warmed solution and stirred at 60 °C for 4 h. The resulting product was then centrifuged at 4500 rpm for 6 min, and the precipitate was redispersed in deionized water (2 mL).

Synthesis of Gap-Tunable and RhB-Modified Au/AuAg Core–Shell Nanostructures

The Ag of the Au/Ag core–shell nanostructures was replaced with Au by galvanic replacement and overgrowth process, and a nanogap of tunable width was created between the gold nanocups and the AuAg alloy shell. The prepared Au/Ag core–shell sample (2 mL) and CTAB (0.7 mL, 0.2 M) were mixed and heated with magnetic stirring at 60 °C for 10 min. Afterwards, the pre-prepared solution A ($HAuCl_4$ (0.08 mL, 0.01 M) and deionized water (1 mL)) and solution B (CTAC (0.2 mL, 0.2 M), AA (0.3 mL, 0.1 M) and deionized water (0.5 mL)) were slowly and alternately injected into the pre-warmed solution and stirred at 60 °C for 4 h. The resulting product was then centrifuged at 4500 rpm for 6 min, and the precipitate was redispersed in deionized water (4 mL). The width of the nanogap was tuned by adjusting the amount of the $HAuCl_4$ from 0.02 to 0.32 mL.

Sample Characterization

The transmission electron microscopy (TEM) images were obtained with a JEOL 2010 operating at 200 kV. Scanning electron microscopy (SEM) observations were performed on a Zeiss Sigma FE-SEM operated at an accelerating voltage of 20 kV. The extinction spectra were measured on a TU-1810 UV–Vis spectrophotometer. The SERS spectra were acquired with the laser source with a wavelength of 633 nm (1 mW) for 10 s of illumination on a HORIBA XploRA Plus Raman microscope.

Results and Discussion

We prepared RhB-mediated Au/AuAg core–shell nanostructures based on gold nanocups by a controlled galvanic replacement and overgrowth process. Due to the excellent magnetic plasma properties of gold nanocups, Au/AgAu core–shell nanostructures have tunable plasmon resonance peaks and different widths of nanogaps, and their SERS properties are dependent on the gap width and

the thickness of the alloy shell. The detailed preparation process is shown in Fig. 1a. First, we used gold nanocups (Fig. 1b) that were obtained by selective growth of Au on PbS nanooctahedra and subsequent selective dissolution of the PbS component) as a starting substrate. Au/Ag core–shell nanostructures were synthesized by adding the precursor $AgNO_3$ and the reducing agent AA. Figure 1c shows the SEM image of Au/Ag core–shell nanostructures with 0.08 mL $AgNO_3$ added. As the amount of $AgNO_3$ added increased, the opening in the gold nanocups was gradually filled by Ag, and the Ag shell layer on the outside of the gold nanocups becomes thicker. RhB-mediated Au/Ag core–shell nanostructures which were added with the amount of $AgNO_3$ of 0.08 mL were chosen as the substrate. Then, Au/AgAu core–shell nanostructures with the RhB molecules embedded in the nanogap were obtained via a galvanic replacement and overgrowth process by adding $HAuCl_4$ and the reducing agent AA. Figure 1d shows the SEM image of Au/AgAu core–shell nanostructures when the molar ratio of Au to Ag is 4:1. In Fig. 1(e), the EDS energy spectrum of Au/AgAu core-shell nanostructures with the molar ratio of 1:1 between Au and Ag.

In order to clearly observe the change regular of the gap widths with a different molar ratio of Au to Ag, Fig. 2 shows a set of representative TEM images of Au/AgAu core–shell nanostructures with different gap widths. The amount of $HAuCl_4$ added was controlled by regulating the molar ratio of Au to Ag ($HAuCl_4$: $AgNO_3$), replacing the Ag shell with Au to form an AuAg alloy shell and nanogap. In particular, the gap widths were turned from ~ 7.4 to ~ 3.2 nm by increasing the molar ratio of Au to Ag from 1:2 to 2:1 (insets in Fig. 2a–c).

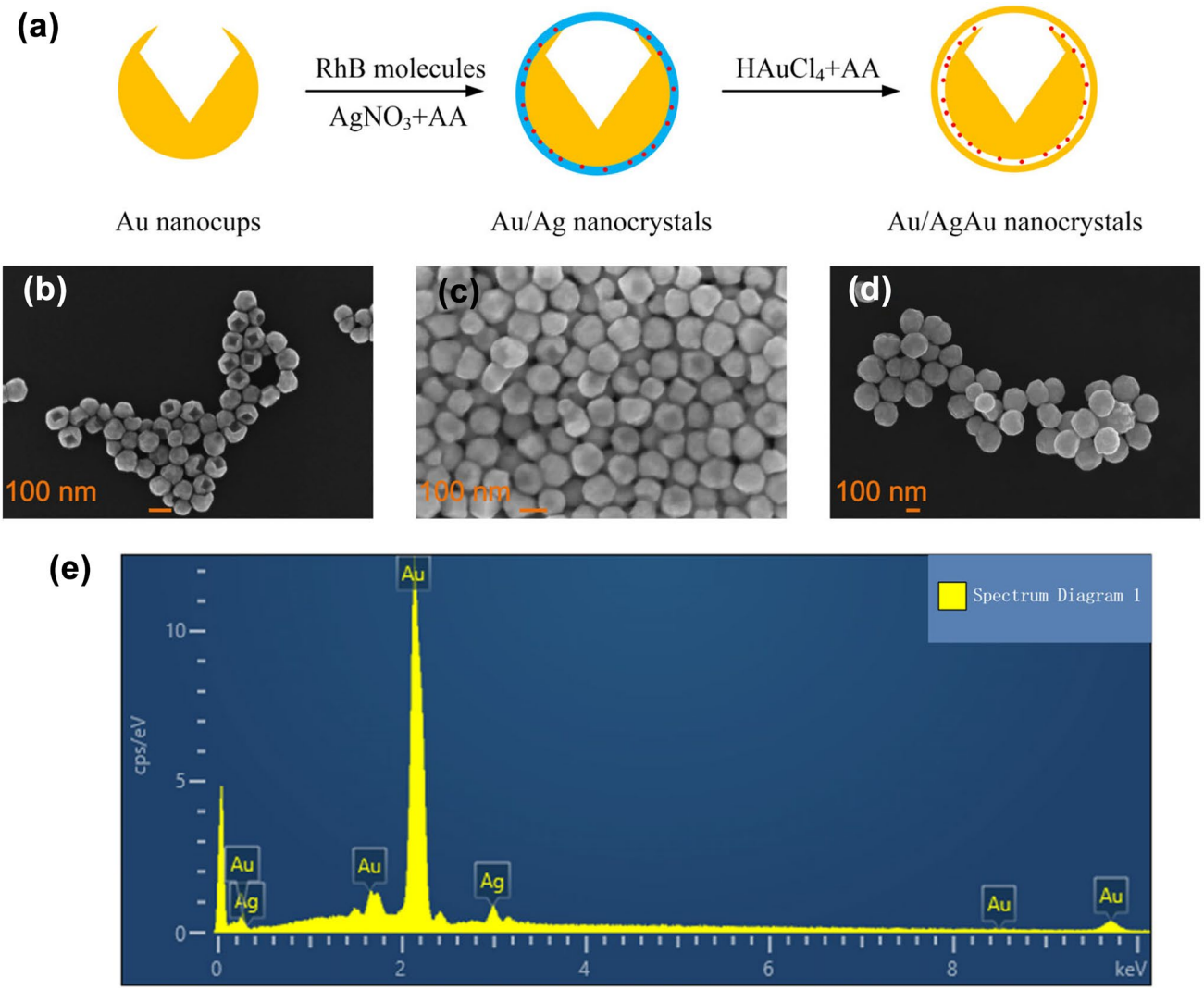

Fig. 1 **a** Schematic illustration of the synthesis process of RhB-mediated Au/AgAu core–shell nanostructures. **b–d** SEM images of gold nanocups, Au/Ag core–shell nanostructures with 0.08 mL $AgNO_3$, and Au/AuAg core–shell nanostructures with the molar ratio of 4:1 between Au and Ag. **e** EDS energy spectrum of Au/AgAu core–shell nanostructures with the molar ratio of 1:1 between Au and Ag

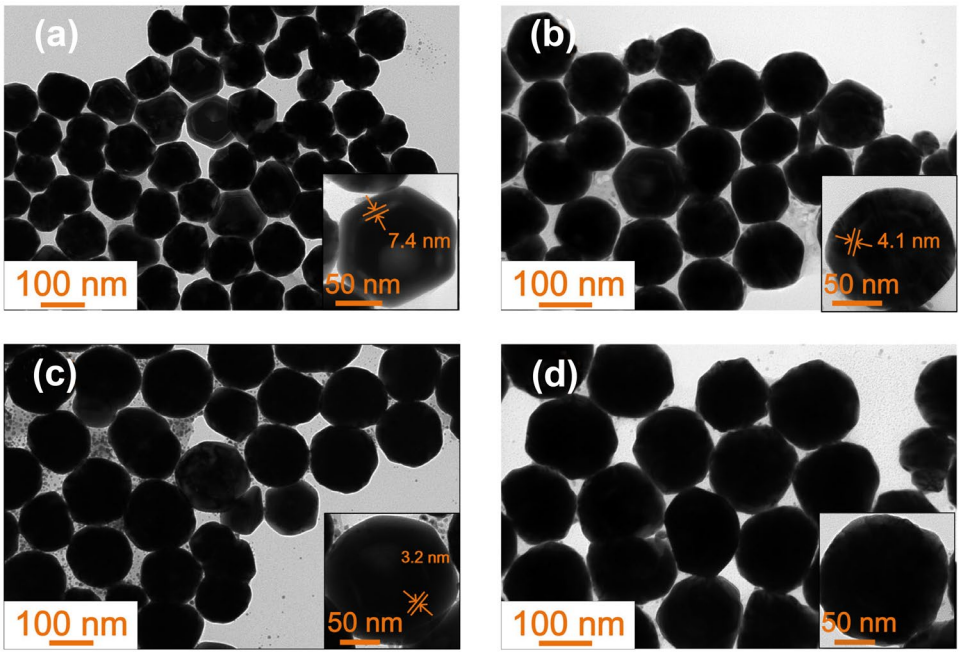

Fig. 2 TEM images of Au/AgAu core–shell nanostructures with different gap widths: ~ 7.4 nm (**a**), ~ 4.1 nm (**b**), ~ 3.2 nm (**c**), and unmeasurable (**d**). The corresponding molar ratio of Au to Ag is 1:2, 1:1, 2:1, and 4:1

When the molar ratio of Au to Ag is greater than 2:1, the nanogap could hardly be observed due to the large thickness of the alloy shell (Fig. 2d). These Au/AgAu core–shell nanostructures with adjustable gap widths provided a good platform for gap-enhanced SERS based on magnetic plasmon coupling.

The plasmon resonance of Au/AgAu core–shell nanostructures was studied by extinction spectra. Figure 3a shows the extinction spectra of gold nanocups, RhB-mediated Au/Ag core–shell nanostructures, and RhB-mediated Au/Ag core–shell nanostructures at the same particle concentration. The initial gold nanocups have a magnetic dipole plasmon peak located at 610 nm and the plasmon resonance peak of the RhB-mediated Au/Ag core–shell nanostructures blue shift to 560 nm with 0.08 mL $AgNO_3$ added. The Ag shell layer significantly changed the plasmon resonance mode of gold nanocups. As the amount of $AgNO_3$ added increased from 0.01 to 0.15 mL, the plasma peak blue shifted from 593 to 553 nm, and a new peak gradually appeared at 425 nm, which was attributed to the effect of the Ag shell on the dielectric constant of the Au core. When excessive amounts of $AgNO_3$ were added, no more Ag could be deposited on the surface of gold nanocups, and the remaining Ag nucleated itself in solution to form Ag nanospheres. The extinction spectra of the RhB-mediated Au/AgAu core–shell nanostructures with different molar ratios of Au to Ag are shown in Fig. 3b. As the molar ratio of Au to Ag increased from 1:4 to 4:1, the plasmon resonance peak of the RhB-mediated Au/AgAu core–shell nanostructures was red-shifted from 580 to 721 nm, and a shoulder peak appeared at 550 nm to the left of the main plasmon resonance peak when the molar ratio of Au to Ag was greater than 1:1, with a gradual increase in intensity and a slight red-shift as the molar ratio of Au to Ag increased. During the galvanic replacement process, the AuAg alloy shell thickness gradually becomes thicker and the gap width gradually becomes smaller of Au/AgAu core–shell nanostructures as the molar ratio of Au to Ag continued to increase. A strong plasma coupling could be induced in the nanogap, resulting in a strong local electromagnetic field. These Au/AgAu core–shell nanostructures with tunable plasmon resonance peak offer the possibility to enhance the Raman signals.

The SERS properties of RhB-embedded Au/AgAu core–shell nanostructures with different molar ratios of Au to Ag were tested under excitation at 633 nm which matched well with the magnetic plasmon resonance peak, and the results are shown in Fig. 4a. The Raman spectra of the RhB molecules can be clearly observed, indicating that the RhB molecules were well embedded in the nanogaps. The SERS peaks at 1360 cm^{-1} and 1647 cm^{-1} are referred to as the C–C stretching mode. It is noteworthy that the Raman intensity of the Au/AgAu core–shell nanostructures increases dramatically as the Au–Ag molar ratio increases from 1:4 to 2:1 but then decreases dramatically when the Au–Ag molar ratio reaches 4:1. The characteristic peaks at 1350 cm^{-1} and 1275 cm^{-1} are used as the standard peaks for comparing the SERS performance of the Au/AgAu core–shell nanostructures. As shown in Fig. 4b, the Au/AgAu core–shell nanostructures with the molar ratio of 2:1 between Au and Ag have the highest Raman intensity, which is ~ 12 times higher than Au/AgAu core–shell nanostructures with the molar ratio is 1:4, of Au to Ag at 1350 cm^{-1}, and ~ 11 times at 1275 cm^{-1}, respectively. The gap

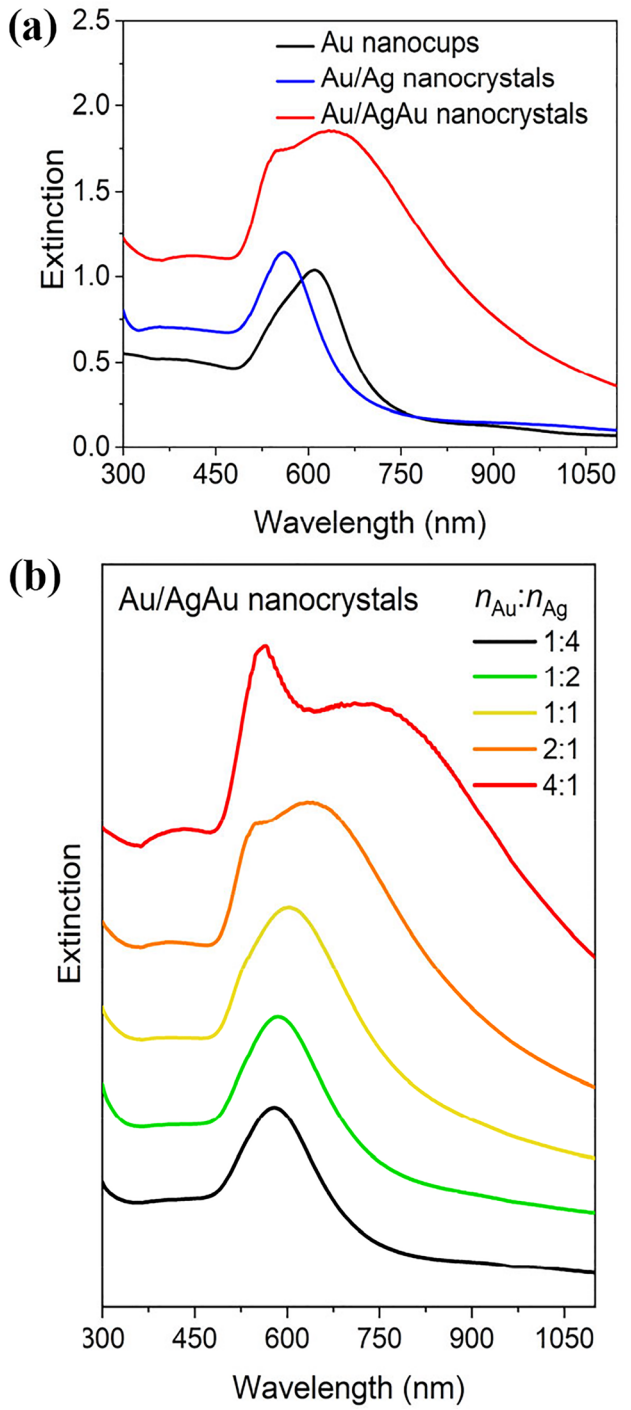

Fig. 3 **a** Experimental extinction spectra of gold nanocups, Au/Ag core–shell nanostructures with 0.08 mL $AgNO_3$ added, and Au/AgAu core–shell nanostructures with the molar ratio of 2:1 between Au and Ag. **b** Experimental extinction spectra of Au/AgAu core–shell nanostructures with different molar ratios of Au to Ag

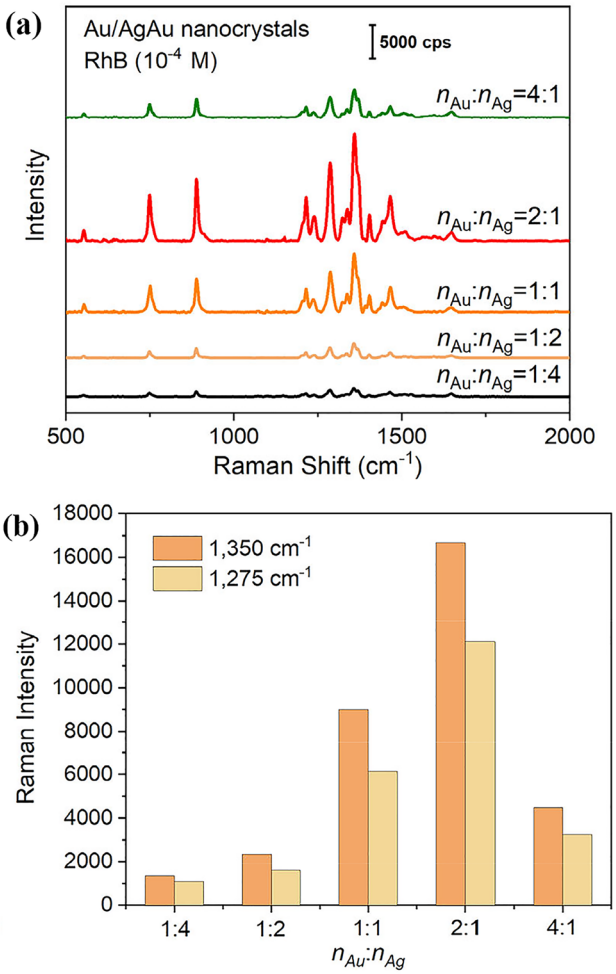

Fig. 4 **a** Raman spectra of Au/AgAu core–shell nanostructures with different molar ratios of Au to Ag. **b** Raman intensity at 1360 cm^{-1} and 1275 cm^{-1} of RhB-embedded Au/AgAu core–shell nanostructures with different molar ratios of Au to Ag

width of Au/Ag core–shell nanostructures decreased with the molar ratio of Au to Ag increased. When the molar ratio of Au to Ag was 2:1, the gap width was extremely small relative to the alloy shell thickness, and the Raman excitation wavelength (633 nm) was well matched to the magnetic plasma resonance peak position of Au/Ag core–shell nanostructures; therefore, the highest Raman signals were obtained. When the molar ratio of Au to Ag is greater than 2:1, the alloy shell has become thicker to reduce the penetration and scattering of light, causing the Raman signals strength to drop sharply. The results offer potential strategies for enhancing the SERS performance.

Conclusions

In summary, RhB-embedded Au/AgAu core–shell nanostructures with tunable gap widths were synthesized via controlled galvanic replacement and overgrowth process based on gold nanocups, to achieve tunable amplified Raman signals with different gap widths. The RhB molecules could be coupled to gold nanocups which had strong magnetic

plasmon properties by soaking the gold nanocups in an aqueous RhB solution. Au/AgAu core–shell nanostructures showed prominent plasmon absorption and strong local electromagnetic field enhancement owing to the synergistic effect of electromagnetic plasmon resonance and plasmon coupling. In particular, Au/AgAu core–shell nanostructures with the molar ratio is 2:1 of Au to Ag show the highest SERS activity; this may be due to the plasmon resonance peak position of the sample matches well with the Raman excitation wavelength (633 nm), and the width of the nanogap is small enough to result in strong electromagnetic coupling. And when the molar ratio of Au to Ag is greater than 2:1, the shielding effect of the thicker alloy shell will weaken the Raman signals considerably. Our findings provide a new possibility for synthesize gap-enhanced Raman tags based on magnetic plasma coupling for enhancing the Raman performance.

Author Contribution Sample preparation, data collection, and analysis were performed by Zhirui Zhao and Shuo Zhang. The first draft of the manuscript was written by Zhirui Zhao, and all authors commented on previous versions of the manuscript. All authors read and approved the final manuscript.

Funding This research was funded by Hubei Key Laboratory of Optical Information and Pattern Recognition by the Wuhan Institute of Technology (202004 and 202010), the National Natural Science Foundation of China (12274379, 11904332 and 11904270), and Zhejiang Provincial Natural Science Foundation of China under grant no. LQQ20A040001.

Data Availability Informed consent was obtained from all subjects involved in the study. The data presented in this study are available on request from the corresponding author.

Declarations

Conflict of Interest The authors declare no competing interests.

References

1. Kurouski D, Large N, Chiang N, Henry A, Seideman T, Schatz GC, Van Duyne RP (2017) Unraveling near- and far-field relationship of 2D SERS substrates using wavelength-scan surface-enhanced Raman excitation spectroscopy. J Phys Chem C 121:14737–14744. https://doi.org/10.1021/acs.jpcc.7b04787
2. Zhao YQ, Xue MF, Göransson DJO, Borgström MT, Xu HQ, Chen JN (2021) Probing strain in wurtzite InP-InAs core-shell nanowires with Raman spectroscopy. Phys Rev B 104:235309. https://doi.org/10.1103/PhysRevB.104.235309
3. Chen N, Rong M, Shao XG, Zhang H, Liu SP, Dong BJ, Xue W, Wang TY, Li TH, Pan JH (2017) Surface-enhanced Raman spectroscopy of serum accurately detects prostate cancer in patients with prostate-specific antigen levels of 4–10 ng/mL. Int J Nanomedicine 12:5399–5407. https://doi.org/10.2147/IJN.S137756
4. Hagiwara Y, Sogo Y, Takahata K, Yamamoto J (2018) Temperature dependence of CO2 densimetry using micro-Raman spectrometry at laboratory conditions. Geochem J 52:379–383. https://doi.org/10.2343/geochemj.2.0523
5. Poliani E, Wagner MR, Reparaz JS, Mandl M, Strassburg M, Kong X, Trampert A, Sotomayor Torres CM, Hoffmann A, Maultzsch J (2013) Nanoscale imaging of InN segregation and polymorphism in single vertically aligned InGaN/GaN multi quantum well nanorods by tip-enhanced Raman scattering. Nano Lett 13:3205–3212. https://doi.org/10.1021/nl401277y
6. Le Ru EC, Etchegoin PG (2012) Single-molecule surface-enhanced Raman spectroscopy. Annu Rev Phys Chem 63:65–87. https://doi.org/10.1146/annurev-physchem-032511-143757
7. Faulds K, Graham D, Smith WE (2004) Evaluation of surface enhanced resonance Raman scattering for quantitative DNA analysis. Anal Chem 76:412–417. https://doi.org/10.1021/ac035060c
8. Müller M, Rinia HA, Bonn M (2006) Quantitative multiplex CARS spectroscopy in congested spectral regions. J Phys Chem B 110:4472–4479. https://doi.org/10.1021/jp0564849
9. Li CC, Huang YM, Li XY, Zhang YR, Chen QL, Ye ZW, Alqarni Z, Bell SEJ, Xu YK (2021) Towards practical and sustainable SERS: a review of recent developments in the construction of multifunctional enhancing substrates. J Mater Chem C 9:11517–11552. https://doi.org/10.1039/D1TC02134F
10. Alessandri I, Lombardi JR (2016) Enhanced Raman scattering with dielectrics. Chem Rev 116:14921–14981. https://doi.org/10.1021/acs.chemrev.6b00365
11. Chen G, Wang Y, Yang M (2010) Measuring ensemble-averaged surface-enhanced Raman scattering in the hotspots of colloidal nanoparticle dimers and trimers. J Am Chem Soc 132:3644–3645. https://doi.org/10.1021/ja9090885
12. Zhang Z, Xu F, Yang WA (2011) Facile one-pot method to high-quality Ag-graphene composite nanosheets for efficient surface-enhanced Raman scattering. ChemComm 47:6440–6442. https://doi.org/10.1039/C1CC11125F
13. Choi J, Kim J, Oh J (2019) Surface-enhanced Raman scattering-based detection of hazardous chemicals in various phases and matrices with plasmonic nanostructures. Nanoscale 11:20379–20391. https://doi.org/10.1039/C9NR07439B
14. Ly NH, Joo SW (2020) Recent advances in cancer bioimaging using a rationally designed Raman reporter in combination with plasmonic gold. J Mater Chem B 8:186–198. https://doi.org/10.1039/C9TB01598A
15. Zhang R, Zhang Y, Dong ZC, Jiang S, Zhang C, Chen G, Zhang L, Liao Y, Aizpurua J, Luo Y, Yang JL, Hou JG (2013) Chemical mapping of a single molecule by plasmon-enhanced Raman scattering. Nature 498:82–86. https://doi.org/10.1038/nature12151
16. Lu G, Yuan H, Su L, Kenens B, Fujita Y (2017) Plasmon-mediated surface engineering of silver nanowires for surface-enhanced Raman scattering. J Phys Chem Lett 8:2774–2779. https://doi.org/10.1021/acs.jpclett.7b00958
17. Wu Y, Wang X, Wen X (2020) Surface-enhanced Raman scattering based on hybrid surface plasmon excited by Au nanodisk and Au film coupling structure. Phys Lett A 384:126544. https://doi.org/10.1016/j.physleta.2020.126544
18. Kassim S, Mukhtar NA, Tahrin RAA (2020) Synthesis and characterization of plasmon-enhanced SERS substrate based on Au-Ag alloy-coated, large-area photonic (methyl methacrylate + styrene) co-polymer. Mater Sci Forum 982:14–19. https://doi.org/10.4028/www.scientific.net/MSF.982.14
19. Schmid T, Opilik L, Blum C (2013) Nanoscale chemical imaging using tip-enhanced Raman spectroscopy: a critical review. Angew Chem Int Ed 52:2–17. https://doi.org/10.1002/anie.201203849
20. Lafuente M, Pellejero I, Clemente A (2020) In-situ synthesis of SERS active Au@POM nanostructures in a microfluidic device for real time detection of water pollutants. ACS Appl Mater Interfaces 12:36458–36467. https://doi.org/10.1021/acsami.0c06725
21. Zhang SR, Jiang RB, Guo YZ, Yang BC, Chen XL, Wang JF, Zhao YF (2016) Plasmon modes induced by anisotropic gap

opening in Au@Cu2O nanorods. Small 12:4264–4276. https://doi.org/10.1002/smll.201600065
22. Sandu T (2012) Shape effects on localized surface plasmon resonances in metallic nanoparticles. J Nanopart Res 14:905. https://doi.org/10.1007/s11051-012-0905-6
23. Li P, Yan X, Zhou F (2017) A capillary force-induced Au nanoparticle-Ag nanowire single hot spot platform for SERS analysis. J Mater Chem C 5:3229–3237. https://doi.org/10.1039/C7TC00150A
24. Raveendran J, Docoslis A (2021) Detection and quantification of toxicants in food and water using Ag-Au core-shell fractal SERS nanostructures and multivariate analysis. Talanta 231:122383. https://doi.org/10.1016/j.talanta.2021.122383
25. Jiji SG, Gopchandran KG (2017) Au-Ag hollow nanostructures with tunable SERS properties. Spectrochim Acta A Mol Biomol Spectrosc 171:499–506. https://doi.org/10.1016/j.saa.2016.08.022
26. Nair S, Gomez-Cruz J, Ascanio G, Docoslis A, Sabat RG, Escobedo C (2021) Escobedo C. Cicada Wing inspired template-stripped SERS active 3D metallic nanostructures for the detection of toxic substances. Sensors 21:1699. https://doi.org/10.3390/s21051699
27. Metiu H (1984) Surface enhanced spectroscopy. Prog Surf Sci 17:153–320. https://doi.org/10.1016/0079-6816(84)90017-0
28. Zhang Q, Large N, Nordlander P, Wang H (2014) Porous Au nanoparticles with tunable plasmon resonances and intense field enhancements for single-particle SERS. J Phys Chem Lett 5:370–374. https://doi.org/10.1021/jz402795x
29. Zong C, Xu MX, Xu LJ, Wei T, Ma X, Zheng XS, Hu R, Ren B (2018) Surface-enhanced Raman spectroscopy for bioanalysis: reliability and challenges. Chem Rev 118:4946–4980. https://doi.org/10.1021/acs.chemrev.7b00668
30. Hamon C, Liz-Marzán LM (2018) Colloidal design of plasmonic sensors based on surface enhanced Raman scattering. J Colloid Interface Sci 512:834–843. https://doi.org/10.1016/j.jcis.2017.10.117
31. Xu HX, Bjerneld EJ, Käll M, Börjesson L (1999) Spectroscopy of single hemoglobin molecules by surface enhanced Raman scattering. Phys Rev Lett 83:4357–4360. https://doi.org/10.1103/PhysRevLett.83.4357
32. Ding SJ, Ma L, Feng JR, Chen YL, Yang DJ, Wang QQ (2022) Surface-roughness-adjustable Au nanorods with strong plasmon absorption and abundant hotspots for improved SERS and photothermal performances. Nano Res 15:7. https://doi.org/10.1007/s12274-021-3740-1
33. Lin S, Lin X, Liu YL, Zhao HY, Hasi W, Wang L (2018) Self-assembly of Au@Ag core-shell nanocubes embedded with internal standard for reliable quantitative SERS measurements. Anal Methods 10:42014208. https://doi.org/10.1039/C8AY01369A
34. Ye ZX, Lin L, Tan ZY, Zeng YJ, Ruan SC, Ye J (2019) Sub-100 nm multi-shell bimetallic gap-enhanced Raman tags. Appl Surf Sci 487:1058–1067. https://doi.org/10.1016/j.apsusc.2019.05.200
35. Jiang S, Zhang Y, Zhang R, Hu CR, Liao MH, Luo Y, Yang JL, Dong ZC, Hou JG (2015) Distinguishing adjacent molecules on a surface using plasmon-enhanced Raman scattering. Nat Nanotechnol 10:865–869. https://doi.org/10.1038/nnano.2015.170
36. Wei H, Xu H (2013) Hot spots in different metal nanostructures for plasmon-enhanced Raman spectroscopy. Nanoscale 5:10794–10805. https://doi.org/10.1039/C3NR02924G
37. Su J, Wang D, Nörbel L, Shen JL, Zhao ZH, Dou YZ, Peng TH, Mathur S, Fan CH, Song SP (2017) Multicolor gold-silver nanomushrooms as ready-to-use SERS probes for ultrasensitive and multiplex DNA/miRNA detection. Anal Chem 89:2531–2538. https://doi.org/10.1021/acs.analchem.6b04729
38. Nikov RG, Nedyalkov NN, Atanasov PA, Hirsch D, Rauschenbach B, Grochowska K, Sliwinski G (2016) Characterization of Ag nanostructures fabricated by laser-induced dewetting of thin films. Appl Surf Sci 374:36–41. https://doi.org/10.1016/j.apsusc.2015.09.004
39. Ma L, Chen YL, Yang DJ, Ding SJ, Xiong L, Qin PL, Chen XB (2020) Gap-dependent plasmon coupling in Au/AgAu hybrids for improved SERS performance. J Phys Chem C 124:25473–25479. https://doi.org/10.1021/acs.jpcc.0c07701
40. Zhang Y, Yang P, Muhammed MA, Alsaiari SK, Moosa B, Almalik A, Ringe E, Khashab NM (2017) Tunable and linker free nanogaps in core-shell plasmonic nanorods for selective and quantitative detection of circulating tumor cells by SERS. ACS Appl Mater Interfaces 9:37597–37605. https://doi.org/10.1021/acsami.7b10959
41. Zhao Y, Zheng F, Ke W, Zhang W, Shi XL, Liu H (2019) Gap-tethered Au@AgAu Raman tags for the ratiometric detection of MC-LR. Anal Chem 91:7162–7172. https://doi.org/10.1021/acs.analchem.9b00348
42. Nam JM, Oh JW, Lee H, Suh YD (2016) Plasmonic nanogap-enhanced Raman scattering with nanoparticles. Acc Chem Res 49:2746–2755. https://doi.org/10.1021/acs.accounts.6b00409
43. Wu HY, Choi CJ, Cunningham BT (2012) Plasmonic nanogap-enhanced Raman scattering using a resonant nanodome array. Small 8:2878–2885. https://doi.org/10.1002/smll.201200712
44. Ma C, Gao QQ, Hong W, Fan J, Fang JX (2016) Real-time probing nanopore-in-nanogap plasmonic coupling effect on silver supercrystals with surface-enhanced Raman spectroscopy. Adv Funct Mater 27:1603233. https://doi.org/10.1002/adfm.201603233
45. Yang C, Chen Y, Liu D, Chen C, Wang JM, Fan Y, Huang SM, Lei WW (2018) Nanocavity-in-multiple nanogap plasmonic coupling effects from vertical sandwich-like Au@Al2O3@Au arrays for surface-enhanced Raman scattering. ACS Appl Mater Interfaces 10:8317–8323. https://doi.org/10.1021/acsami.7b17228
46. Lin L, Zhang Q, Li XY, Qiu M, Jiang X, Jin W, Gu HC, Lei DY, Ye J (2018) Electron transport across plasmonic molecular nanogaps interrogated with surface-enhanced Raman scattering. ACS Nano 12:6492–6503. https://doi.org/10.1021/acsnano.7b08224
47. Jiang RB, Qin F, Liu YJ, Ling YX, Guo J, Tang MH, Cheng S, Wang JF (2016) Colloidal gold nanocups with orientation-dependent plasmonic properties. Adv Mater 28:6322–6331. https://doi.org/10.1002/adma.201601442